


Research on the Cutting Performance of Self-Lubricating Tools with Microtexture of the Front and Back Surfaces

Yan Zhang  – Haodong Sun – Qi Li – Kaiming Sun – Yuanjing Mou – Shihong Zhang

Changchun University, School of Mechanical and Vehicle Engineering, China

 220101010@ccu.edu.cn

A novel hexagonal microtexture is proposed to enhance the cutting performance of polycrystalline cubic boron nitride (PCBN) tools. Three-dimensional models of both conventional and microtextured tools are developed, and the turning process is simulated using AdvantEdge finite element software. The effects of cutting force, temperature, and stress on tool performance are investigated. Additionally, microtextured turning tools are fabricated for orthogonal experiments to analyze the effects of different texture positions on cutting performance. When the tools with microstructures on both the rake and flank faces (T4) are used in conjunction with solid lubricants, the cutting force is reduced by 3 % to 7 %. Furthermore, implementation of microtextures decreases the friction coefficient, improves the surface quality of the workpiece, and enhance the tool's wear resistance. Therefore, tools featuring microstructures on both the rake and flank faces, combined with solid lubricants, effectively enhance cutting performance.

Keywords hexagonal microtexture, PCBN tools, turning, finite element simulation, solid lubricant integration

Highlights

- A novel hexagonal microtexture structure is proposed.
- Microtextures are applied to both the rake and flank faces of the cutting tool.
- The cutting performance of microtextured tools at various locations is verified using finite element simulation.
- Cutting performance is analyzed through the synergy of microtextured tools and solid lubricants using orthogonal experiments.

1 INTRODUCTION

Polycrystalline cubic boron nitride (PCBN) is an advanced cutting material that surpasses conventional cubic boron nitride in several key aspects. It exhibits exceptional thermal stability, chemical inertness, and outstanding hardness. Due to these properties, PCBN is widely employed in machining applications for cutting various materials, including bearing steels, high-speed steels, hardened ferrous alloys, superalloys, and wear-resistant cast irons. To enhance machining efficiency, researchers have extensively explored strategies to reduce cutting forces and improve workpiece quality using PCBN tools, yielding valuable scientific insights [1,2].

Microtexturing reduces the tool-chip contact length, thereby minimizing wear and extending tool life [3]. Furthermore, optimizing texturing parameters has been shown to mitigate adverse cutting phenomena, further enhancing machining performance [4]. Patel et al. [5] demonstrated that the micro-grooved texture of carbide inserts significantly affects cutting forces and tool wear during the turning of Ti-6Al-4V titanium alloy. Pan et al. [6] established that microtextured PCBN tools enhance surface quality and wear resistance in the machining of bearing steel GCr15. Rajurkar and Chinchani [7] reported that pit-texture tools achieve superior surface finishes and reduce cutting forces when machining Inconel 718. Li et al. [8] revealed that a microporous texture with an 80 μm diameter exhibits exceptional wear resistance. Feng et al. [9] and Liu et al. [10] determined that well-structured microtextures effectively reduce cutting forces and temperatures. Wang et al. [11] identified abrasive and adhesive wear as the primary wear mechanisms in PCBN tools.

Kumar et al. [12] investigated TiSiVN self-lubricating coatings on $\text{Al}_2\text{O}_3\text{-SiC}$ ceramic tools for the dry cutting of Ti6Al4V alloy. Their findings indicated that the coating effectively reduced friction, wear, surface roughness, and cutting temperatures. Xing et al. [13] utilized

additive manufacturing to develop self-lubricating coatings, where MoS_2 particles formed a lubricating film that significantly decreased friction and wear. Struzikiewicz [14] determined that feed rate and depth of cut were the primary factors influencing cutting forces when employing Prime Turning with high-pressure cooling. Korpysa et al. [15] demonstrated that both tool coating and machining parameters had a substantial impact on surface quality when using TiB₂- and TiAlN-coated carbide end mills. Additionally, coated tools have been shown to enhance tool life and improve surface finish [16-18].

Previous studies have primarily concentrated on the development of surface topographies, such as dimples and grooves, on the rake face of cutting tools, often in combination with self-lubricating coatings. However, there is a significant gap in evaluating the cutting performance of self-lubricating tools that feature microtextures on both the rake and flank faces, particularly when these textures are integrated with solid lubricants. To address this, the present research proposes a novel approach of fabricating hexagonal microtextures on both the rake and flank surfaces of PCBN tools through laser processing, followed by the incorporation of solid lubricants within these microtextures. Finite element analysis and cutting experiments are performed on bearing steel to assess the synergistic effects of microtexturing and solid lubricants on cutting force, surface roughness, and tool wear. The findings provide essential insights into the design and fabrication of tool surface textures to enhance machining performance.

2 METHODS & MATERIALS

2.1 Origin of Bionic Microtexture Structures

Maladen et al. [19] demonstrated that the sandfish lizard possesses the remarkable ability to navigate desert environments in a manner

similar to swimming. Furthermore, the lizard's skin exhibits exceptional abrasion resistance and low-friction properties against sand, outperforming even steel. While the epidermal scales of the sandfish lizard appear smooth at the macroscopic level, they reveal a complex, non-smooth microstructure under closer inspection. These specialized non-smooth epidermal scales have evolved as adaptations to the harsh conditions of the sandfish lizard's habitat, enabling it to thrive over extended periods. This study analyzes the configuration of the sandfish lizard's surface structures, focusing on the extraction of the hexagonal microtexture, as depicted in Fig. 1.

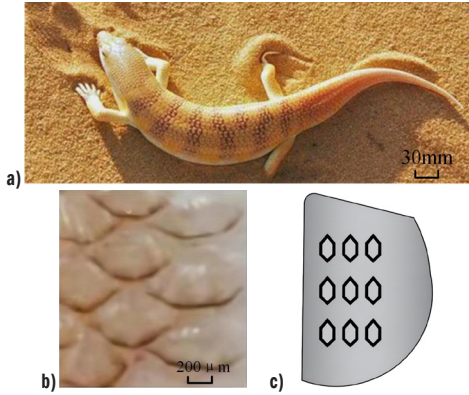


Fig. 1. Source of bionic microtexture structures; a) sandfish lizard; b) epidermal structure; and c) tool microstructure morphology

2.2 Mechanism of Action of Self-Lubricating Cutting Tools

Ge et al. [20] investigated the application of laser-cut micro-groove textures with varying widths on cutting tool surfaces to enhance the penetration of cutting fluids and improve lubrication at the tool-chip interface. As illustrated in Figs. 2 and 3, the friction surfaces of conventional cutting tools typically come into direct contact, resulting in a dry friction state that exacerbates wear at the contact points.

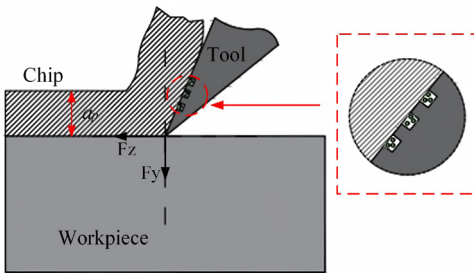


Fig. 2. Mechanism of surface microstructure action

In contrast, the introduction of microtextured structures facilitates the entry of chips into the grooves, thereby alleviating secondary cutting forces and promoting the expulsion of solid lubricants. As

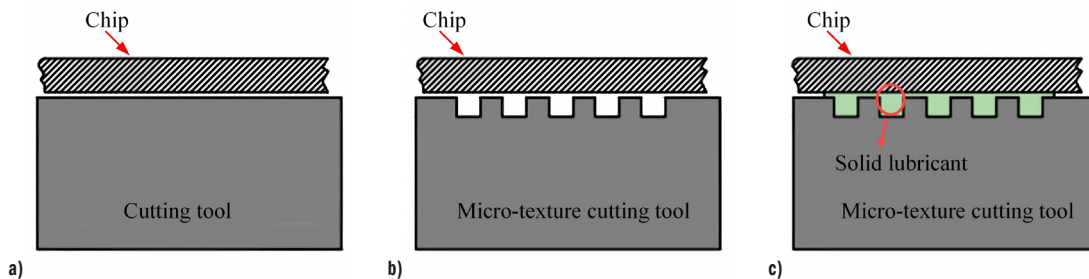


Fig. 3. Mechanism of action of self-lubricating cutting tools, a) traditional tool; b) micro-textured tool, and c) self-lubricating tool

the machining process progresses, this solid lubricant undergoes transformation due to increased temperature and pressure, leading to the formation of a lubricant film that adheres to the insert surface. This mechanism significantly improves lubrication conditions on the tool surface, effectively reducing both friction and wear.

2.3 Establishment of the Cutting Force Model

Fig. 4 presents a simplified model of the microtexturing tool-cutting process. According to metal cutting theory [21], the three-dimensional cutting forces during turning are represented by Eqs. (1) to (4).

$$F_x = a_w L \tau_c \left(\cos \gamma_0 - \frac{\sin \gamma_0}{\tan \beta} \right) \cos(\phi_a + \phi_b), \quad (1)$$

$$F_y = a_w L \tau_c \left(\cos \gamma_0 - \frac{\sin \gamma_0}{\tan \beta} \right) \sin(\phi_a + \phi_b), \quad (2)$$

$$F_z = a_w L \tau_c \left(\sin \gamma_0 + \frac{\sin \gamma_0}{\tan \beta} \right), \quad (3)$$

$$F = \sqrt{F_x^2 + F_y^2 + F_z^2}. \quad (4)$$

where γ_0 is the tool forward tilt angle, ϕ_a is the deflection angle, β is the friction angle, ϕ_b is the chip flow angle, τ_c is the friction shear strength, L is the tool-chip contact length, and a_w is the cutting width.

The actual contact length between the tool and the chip varies as a result of machining the microtexture in the region near the tip and cutting edge of the tool's front face:

$$L' = L - nL_0, \quad (5)$$

where L' is the actual tool-chip contact length, n is the number of textured single edges in the tool-chip contact area, and L_0 is the width of textured single edges in the tool-chip contact area. The actual cutting component forces are represented by Eqs. (6) to (9).

$$F'_x = a_w L' \tau_c \left(\cos \gamma_0 - \frac{\sin \gamma_0}{\tan \beta} \right) \cos(\phi_a + \phi_b), \quad (6)$$

$$F'_y = a_w L' \tau_c \left(\cos \gamma_0 - \frac{\sin \gamma_0}{\tan \beta} \right) \sin(\phi_a + \phi_b), \quad (7)$$

$$F'_z = a_w L' \tau_c \left(\sin \gamma_0 + \frac{\sin \gamma_0}{\tan \beta} \right), \quad (8)$$

$$F' = \sqrt{F'^2_x + F'^2_y + F'^2_z}. \quad (9)$$

Theoretical analysis and derivations presented above clearly demonstrate that the microtextured tool reduces the contact area between the insert and the tool, thereby minimizing cutting forces. Based on these findings, microtextured tools were fabricated, simulated, and experimentally tested in this study.

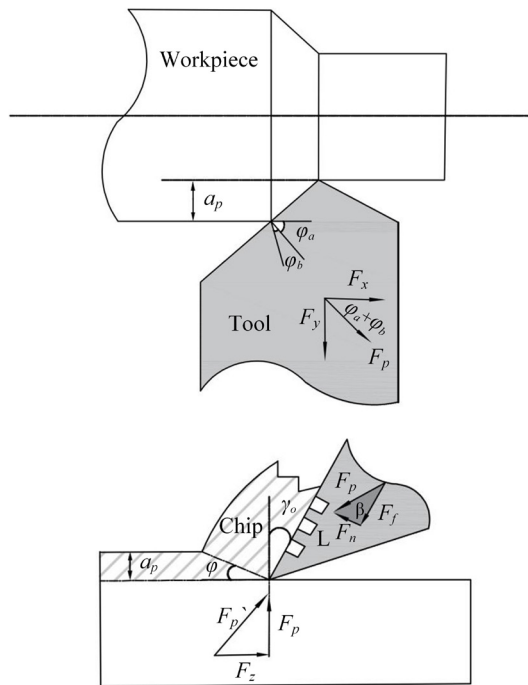


Fig. 4. Simplified model of turning

2.4 Simulation and Analysis of Cutting Performance of Microtexture Tools

2.4.1 Three-Dimensional Modeling of Microtextured Tools

To investigate the influence of various texture placements on cutting performance, microtextures were fabricated on both the front and rear cutting surfaces of the PCBN tool. The tool specifications were as

follows: length and width of 12.73 mm, thickness of 4.76 mm, and a tilt angle of 80° . The texture dimensions included a width of $30\text{ }\mu\text{m}$, a pitch of $100\text{ }\mu\text{m}$, and a depth of $30\text{ }\mu\text{m}$. The workpiece was modeled as a cylindrical component with a diameter of 30 mm and a length of 10 mm . Fig. 5 illustrates the tool dimensions and the three-dimensional model.

2.4.2 Finite Element Simulation Test of Microtextured Tools

In this study, simulation tests were conducted using AdvantEdge finite element software. Table 1 presents the mechanical performance parameters of the PCBN tool, as determined through finite element analysis. The workpiece material employed in the experiments is GCr15 steel, with a hardness rating of 65 HRC. The cutting simulation model, as shown in Fig. 7, utilizes the Lagrangian self-division method for meshing, with a maximum grid size of 0.1 mm and a minimum grid size of 0.02 mm . The simulation procedure, including the turning model, is depicted in Figs. 6 and 7.

Table 1. Mechanical property parameters of PCBN tool for finite element analysis

Young's modulus [GPa]	Thermal conductivity [W/(m·K)]	Poisson's ratio	Density [g/cm ³]	Specific heat capacity [J/(kg·K)]
690	120	0.2	3.8	700

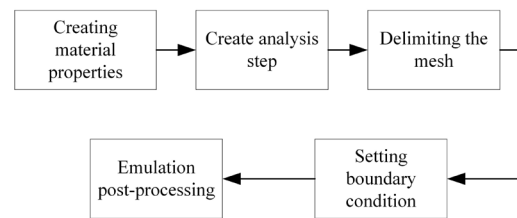


Fig. 6. Cutting simulation process

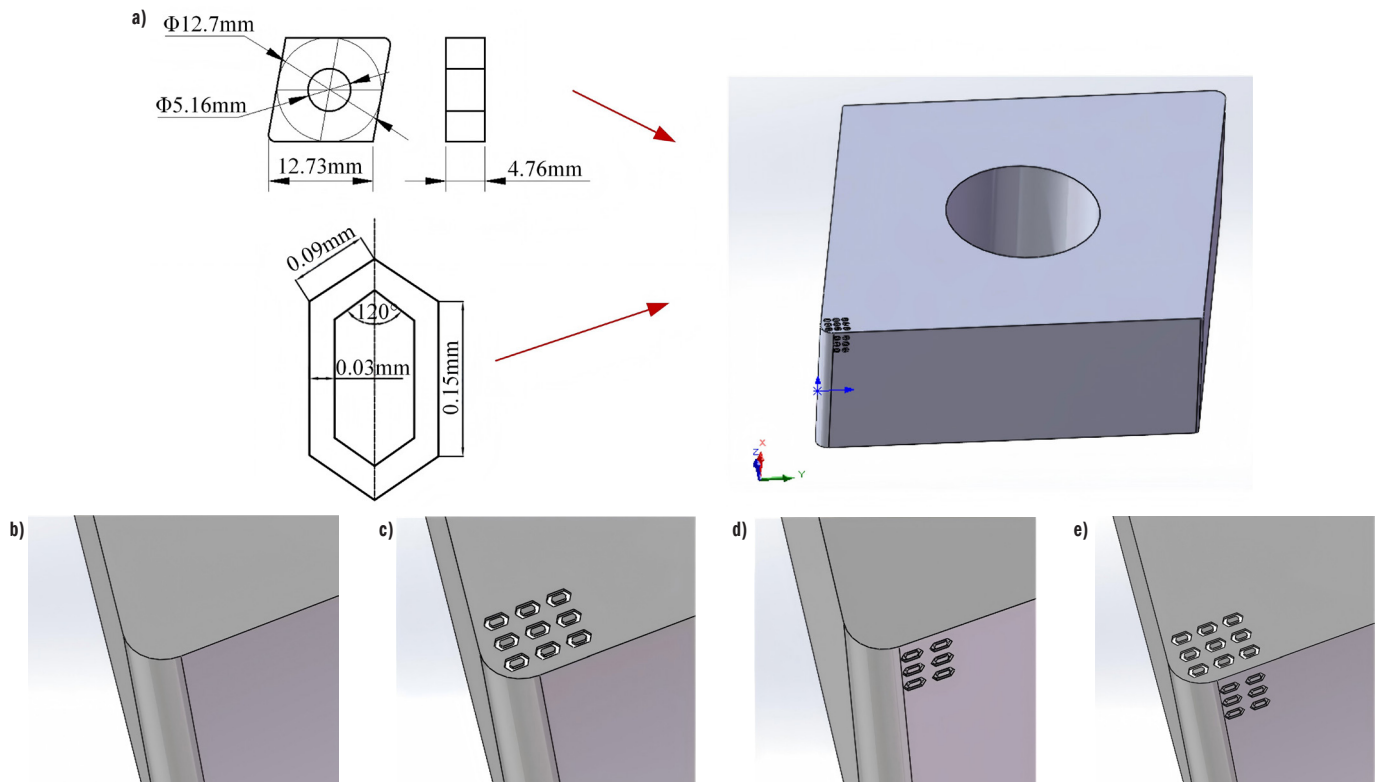


Fig. 5. CNGA120408 tool dimensions and 3D model; a) CNGA120408 tool size; b) T1 tool; c) T2 tool; d) T3 tool; and e) T4 tool

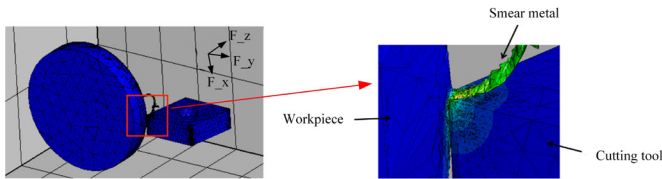


Fig. 7. Simulation flow and cutting model

The mechanical behavior observed during the cutting process was characterized using the Johnson-Cook (J-C) model, which accounts for nonlinear strain hardening and strain rate sensitivity, as expressed in Eq. (10). The parameters relevant to the J-C model for GCr15-bearing steel are provided in Table 2.

Table 2. Parameters of the J-C constitutive equation for GCr15 bearing steel [22]

A [GPa]	B [GPa]	C	m	n
1.67	0.283	0.018	0.88	0.41

$$\bar{\sigma} = [A + B(\bar{\epsilon})^n] \left(1 + C \ln \left(\frac{\dot{\epsilon}}{\dot{\epsilon}_0} \right) \right) \left[1 - \frac{T - T_r}{T_m - T_r} \right]^m \quad (10)$$

where $\bar{\sigma}$ is the material flow stress; A , B , C , m , and n are material constants; $\bar{\epsilon}$ is the equivalent plastic strain; $\dot{\epsilon}$ is the plastic strain rate; $\dot{\epsilon}_0$ is the effective plastic strain rate for quasi-static tests; T is the material temperature; T_r is the reference temperature; and T_m is the melting temperature of the material.

To investigate the effect of texture position on the cutting process, finite element simulations were conducted using T2, T3, and T4 microtextured tools, in addition to the T1 conventional tool. The experimental design is outlined in Table 3.

Table 3. Cutting test program

Group number	Spindle speed V [r/min]	Feed rate f [mm/r]	Back to eat knife a_p [mm]
1	800	0.1	0.1
2	1000	0.15	0.15
3	1250	0.2	0.2

2.4.3 Analysis of Simulation Test Results

During the turning process, the feeding motion of the turning tool generates turning forces, including tangential, radial, and vertical forces. Simultaneously, the high-speed rotation of the workpiece generates substantial heat, which is primarily concentrated at the cutting edge. To evaluate these effects, a finite element analysis was conducted to determine the three components for each group of turning tools. The combined forces were calculated according to Eqs. (4) and (9). Furthermore, the temperature and stress distribution at the tool tip were also analyzed. As illustrated in Fig. 8 to 10, the simulation results reveal that the turning forces, temperature distribution, and stress state exhibit continuous variations depending on the positional configuration of the microtexture structures. First, the microtexture stores chips generated during turning, reducing chip-tool tip contact and tool wear, thereby reducing the turning force. Second, the micro groove enhances heat dissipation by providing additional space, facilitating heat release and reducing the turning temperature.

Influence of front and back face microtexture on cutting forces. Fig. 8 illustrates the cutting force simulation curves for each tool. At a spindle speed of 800 rpm, the average cutting force

is reduced by 16.87 % for tool T4, and by 14.6 % and 5.62 % for tools T2 and T3, respectively, compared to the conventional tool. The reduction in cutting forces can be attributed to the microtextures, which, as indicated by the theoretical analysis, reduce the contact area between the tool and the workpiece, thereby decreasing the cutting force. Among the three sets of simulation results, tool T4 demonstrates the best performance.

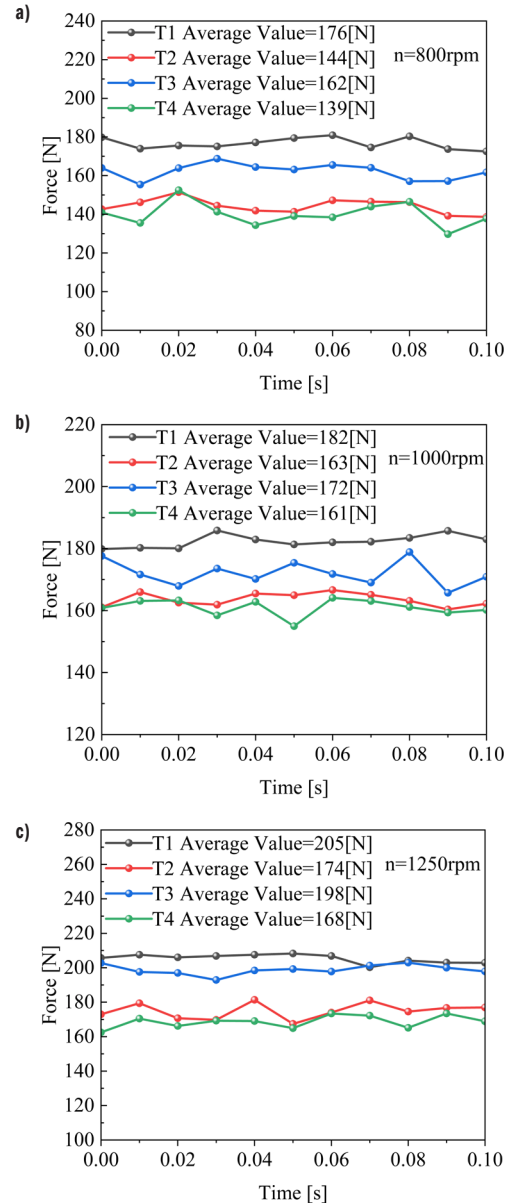


Fig. 8. Cutting forces at different speeds for four tools; a) 800rpm; b) 1000rpm; and c) 1250 rpm

Influence of microtexture on cutting temperature at the front and rear faces. As depicted in Fig. 9, the temperature at the tool tip is observed to be the highest. The thermal energy generated during the cutting process can be attributed to two primary sources: firstly, frictional heat generated by the interaction between the tool, chip, and workpiece, and secondly, the energy consumed in the deformation of the bearing steel. Under identical cutting conditions, biomimetic microtextured tools demonstrate a significantly improved heat dissipation capability compared to conventional tools. This improvement is primarily attributed to additional micro features, which reduce cutting forces by minimizing direct contact between

the tool and the workpiece material. Additionally, the microtexture increases the available surface area for heat dissipation, leading to a subsequent reduction in cutting temperature.

Influence of front and back face microtexture on cutting stresses. The extrusion contact between the workpiece and the cutting edge, which induces elastic-plastic deformation and chipping damage, results in a notable increase in stresses within the cutting zone. Fig. 10 illustrates the distribution of equivalent stress across the surfaces of various tools during the cutting process. The stress attenuation rates for tools T2, T3, and T4 are 10.23 %, 7.45 %, and 15.66 %, respectively, compared to conventional tools. When cutting with tool T1, the average equivalent stress values range between 900 MPa and 1000 MPa, while those for tool T4 are reduced to the range of 800 MPa to 900 MPa. The stresses decrease progressively, with maximum stress concentrations primarily localized in the tip region. Notably, tool T4 demonstrates an 11.1 % reduction in equivalent stress, along with a substantial improvement in the internal stress distribution, when compared to the conventional tool T1.

Finite element simulations conducted on the microtextured tool demonstrated significantly improved performance compared to conventional tools in several key metrics, including cutting forces, stress distribution, and cutting temperature. These results provide a strong basis for the subsequent turning tests and validate the underlying theoretical framework.

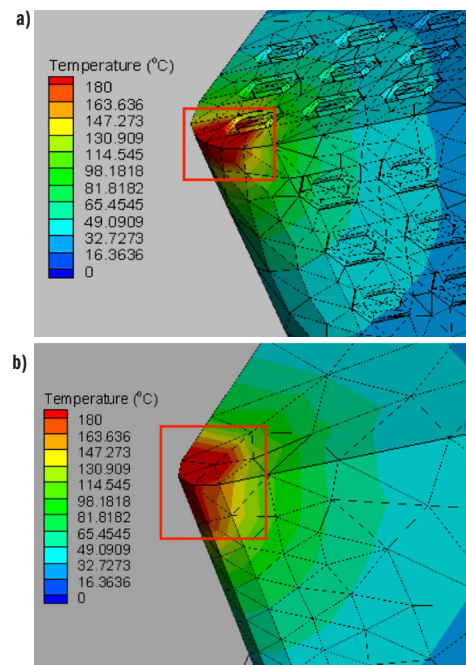


Fig. 9. Tip temperature distribution of tools; a) T4 tool; and b) T1 Tool

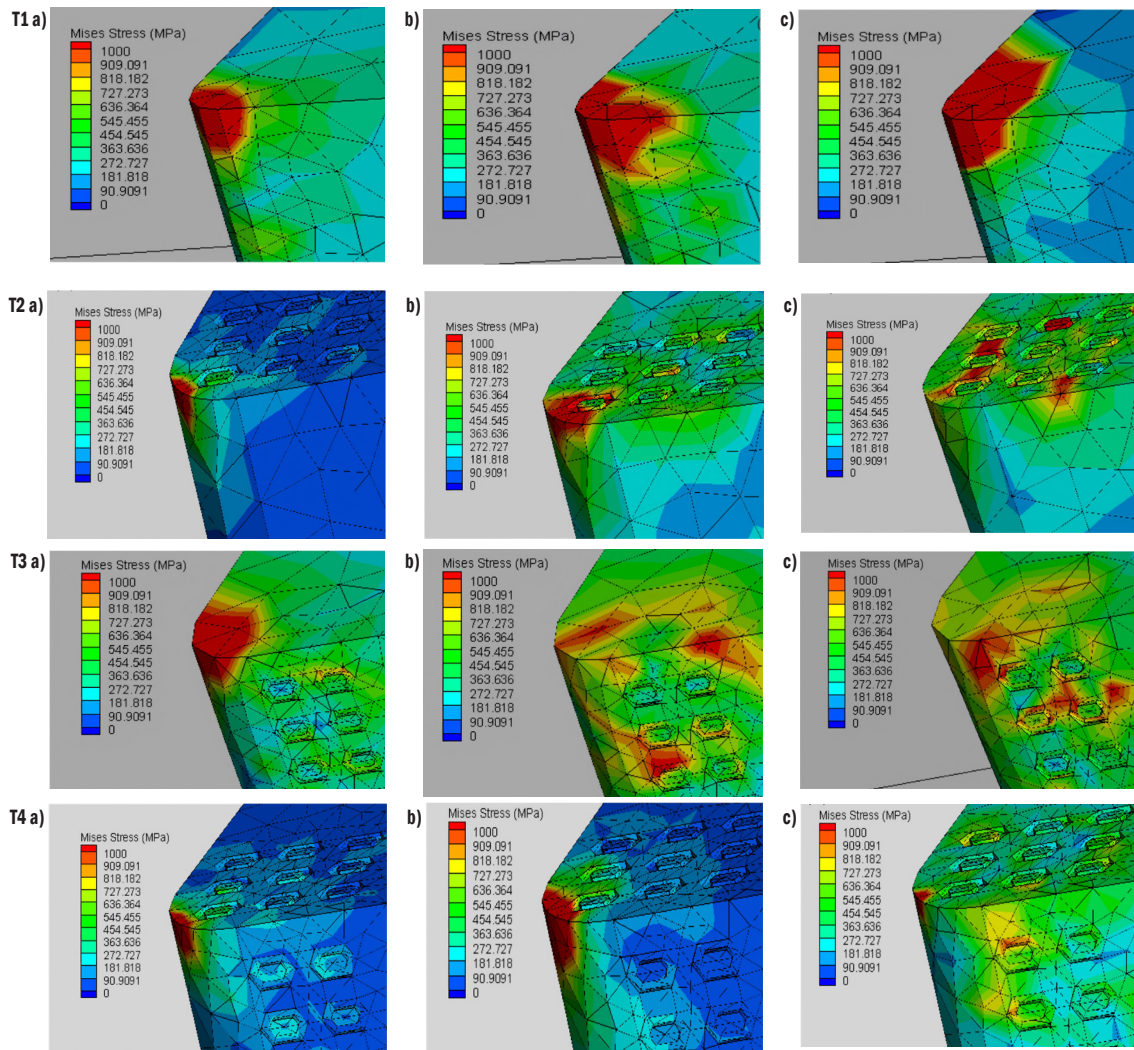


Fig. 10. Stress distribution diagrams of four types of cutting tools over time; a) 0.001s; b) 0.002s; and c) 0.003s

2.5 Experimental Analysis Of Cutting Performance of Microtextured Tools

2.5.1 Microtexture and Solid Lubricant Preparation for Front and Rear Tool Surfaces

In recent years, microtexture machining technology has emerged as a prominent area of research within surface engineering. This technology primarily focuses on creating micro- or nano-scale structures on material surfaces to enhance the cutting performance of tools. Among various methods, laser processing has gained recognition for its high precision, controllability, broad applicability, and environmental sustainability, making it a crucial technique in modern manufacturing. In this study, a ZT-Y-50W YAG laser, provided by Beijing Zhentian Laser Co., Ltd., China, was utilized to fabricate microtextures on the tool surface. Laser processing parameters: spot diameter 0.03 mm, processing speed 60 mm/s, frequency 60 KHz, power 50%, focal length 245 mm, wavelength 1064 nm, number of processes 50. The fabricated hexagonal microtexture featured an edge length of 15 μm , with grooves measuring 30 μm in both depth and width and a spacing of 30 μm between adjacent structures. The surface morphology of the microtexture was analyzed using a Leica DVM2500 super-depth-of-field microscope, as depicted in Fig. 11. Furthermore, Fig. 12 presents the depth profile from the texture edge to the center of the groove, confirming that the groove depth reached 30 μm , in accordance with the established design specifications.

To enhance the cutting performance of microtextured PCBN tools, a solid lubricant composed of molybdenum disulfide (MoS_2) was synthesized by mixing 5000 to 8000 mesh MoS_2 with analytical reagent-grade arsenic trioxide powder in a 1:1 ratio. This solid lubricant was subsequently integrated into the microtextured regions to develop self-lubricating cutting tools. The influence of the lubrication state on the resulting surface quality was then systematically analyzed.

2.5.2 Microtexture Cutting Test for Front and Rear Tool Surfaces

The experiments were performed using a CA6140A machine tool. The cutting tests employed PCBN tools of the CNMG120408 type. The workpiece was composed of GCr15-bearing steel with a diameter of 50 mm and a length of 300 mm. Three-dimensional cutting forces were measured using the DynoWare 2825A-02 force measurement

software and calculated in accordance with Eq. (1). To validate the reliability of the theoretical and simulation results, an orthogonal cutting experimental matrix was designed, as detailed in Table 4.

The static working point fluctuates when the cutter operates within the idle cutting zone, primarily due to temperature variations and an unstable power supply voltage. These fluctuations result in a nonzero cutting force, leading to the zero-drift phenomenon, which introduces variability in the test data. As illustrated in Fig. 13, to mitigate errors associated with zero drift, the average cutting force within the cutting stability interval (sampling interval) was selected as the measurement value. The sampling frequency for the test interval was set at 3000 Hz.

Table 4. Experimental matrix

Group number	Spindle speed V [r/min]	Feed rate f [mm/r]	Back to eat knife a_p [mm]
1	800	0.1	0.1
2	800	0.15	0.2
3	800	0.2	0.15
4	1000	0.1	0.2
5	1000	0.15	0.15
6	1000	0.2	0.1
7	1250	0.1	0.15
8	1250	0.2	0.1
9	1250	0.2	0.2

3 RESULTS AND DISCUSSION

3.1 Effect of Lubricated Tools on Cutting Forces

The radial, axial, and tangential forces were measured using a force gauge, and the total cutting forces were obtained by summing these three directional components. Fig. 14 presents the cutting forces measured during turning experiments under the conditions outlined in Table 3. The results indicate that, compared to the T1 tool, the average cutting forces decreased by 19.8 % for the T4 tool, 16.7 % for the T2 tool, and 11.2 % for the T3 tool, indicating a beneficial effect from the microtextured structure combined with the solid lubricant.

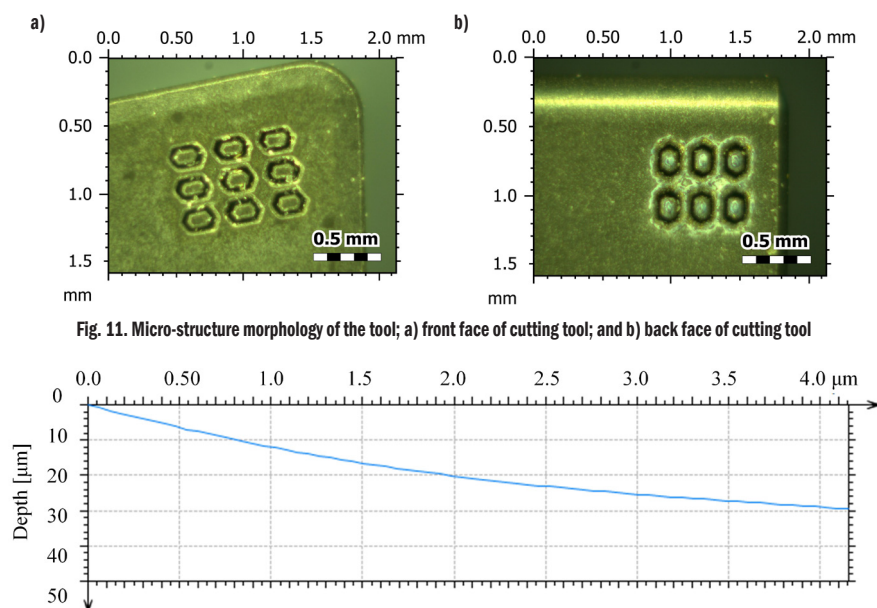


Fig. 11. Micro-structure morphology of the tool; a) front face of cutting tool; and b) back face of cutting tool

Fig. 12. Micro-structure depth profile

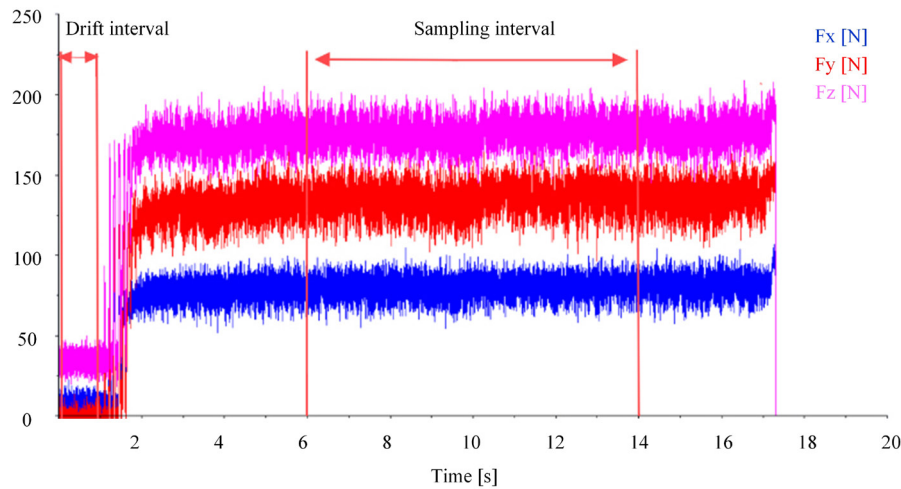


Fig. 13. Distribution of cutting force measurement interval

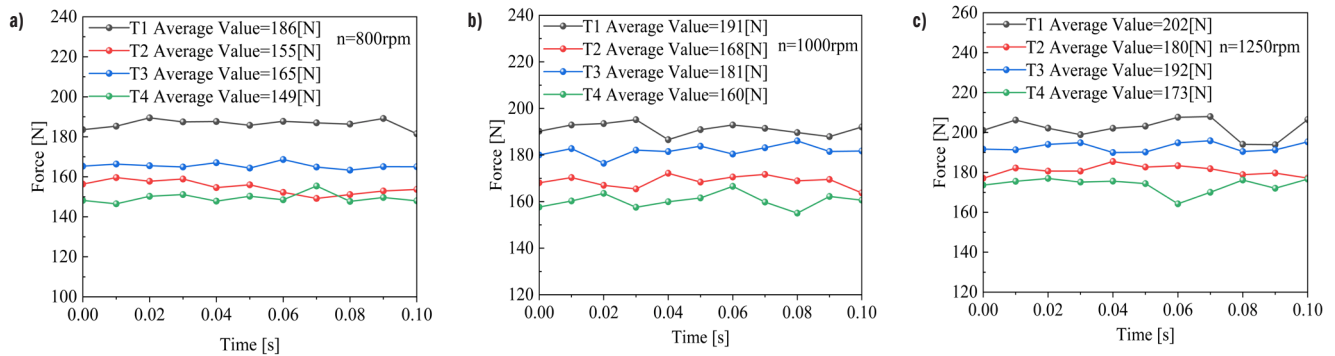


Fig. 14. Cutting forces at different spindle speeds; a) 800 rpm; b) 1000 rpm; and c) 1250 rpm

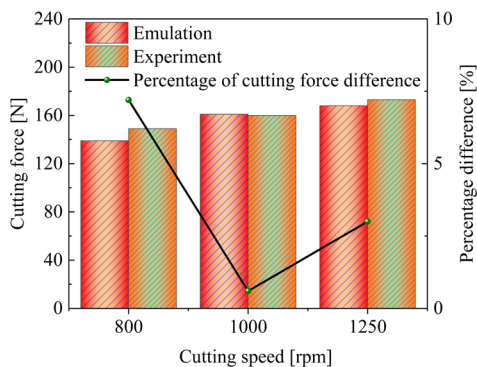


Fig. 15. Comparison of cutting force experiments values and simulation values

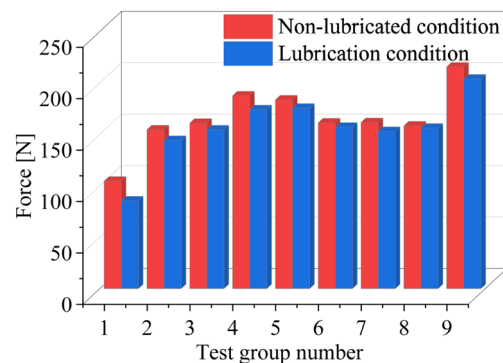


Fig. 16. Comparison of cutting force before and after lubrication

Fig. 15 compares the experimentally measured turning forces of the T4 tool with the simulation data. The error between experimental and simulated data ranged from 1 % to 7 %, which is within an acceptable error range. Additionally, the experimental results of each group demonstrated values slightly higher than the simulation results. This difference arose because the simulation analysis assumes absolutely ideal conditions. However, experimental outcomes in actual processing typically experience influences from factors such as machine tool vibration or environmental temperature changes, leading to an increase in turning force. Furthermore, Fig. 16 compares the cutting forces between the lubricated and non-lubricated conditions for T4 tools, revealing an average reduction of 6.41 %. This result highlights the beneficial synergistic effect of microtexture and solid lubricant on the cutting process.

3.2 Influence of Lubricated Tools on Surface Roughness

Fig. 17a presents a comparative analysis of the surface roughness of bearing steel machined using conventional (T1) and microtextured tools (T2, T3, T4). The T4 tool achieved a surface roughness of 1.51, corresponding to a 37.6 % reduction relative to T1. Surface roughness reductions of 30.6 % and 23.9 % were observed for T2 and T3 respectively. These findings indicate that microtextured tools significantly enhance surface finish, with T4 demonstrating the most pronounced improvement. Fig. 17b further compares test groups 1, 6, and 8, revealing surface roughness reductions of 13.5 %, 6.04 %, and 6.9 % respectively, in comparison to dry cutting. However, minor surface defects, such as pits and scratches, are observed, primarily resulting from tool adhesion deformation. Fig. 18 illustrates the surface morphology of the machined workpiece. The extrusion of

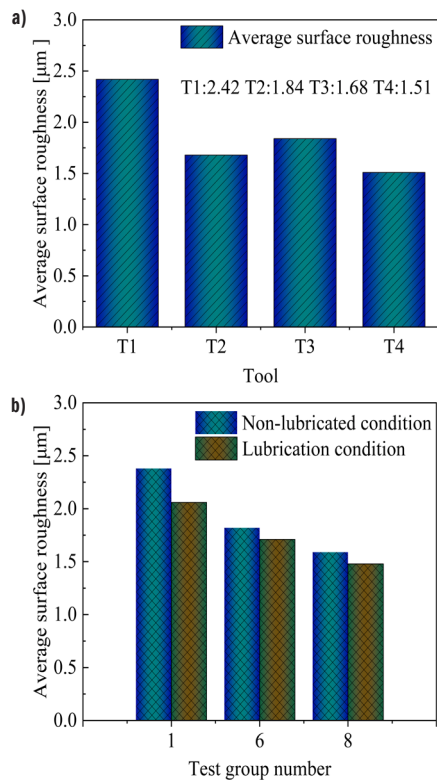


Fig. 17. Comparison of surface roughness; a) surface roughness of workpieces machined using four different cutting tools; and b) surface roughness comparison before and after lubrication

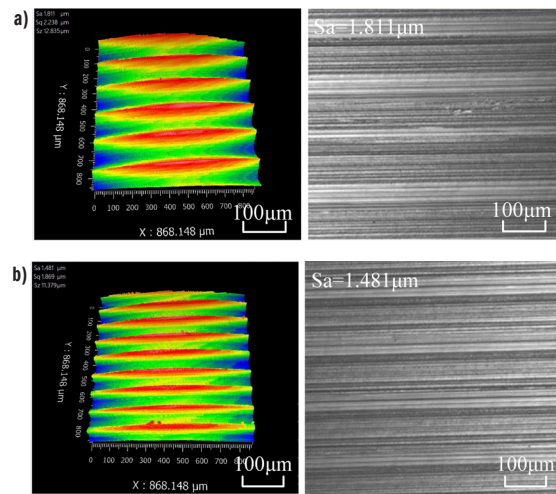


Fig. 18. Comparison of surface morphology before and after lubrication; a) 3D surface topography and profile of the workpiece in dry cutting; and b) 3D surface topography and profile of the workpiece under lubricated conditions

lubricant facilitates the formation of a lubricating film on the contact surface, which enhances wear resistance and improves surface smoothness.

Fig. 18 shows the surface morphology of the workpiece before and after lubrication, where S_a is the area-based arithmetic mean height. The results indicate a reduction in surface roughness following lubrication, along with enhanced wear resistance and improved surface smoothness.

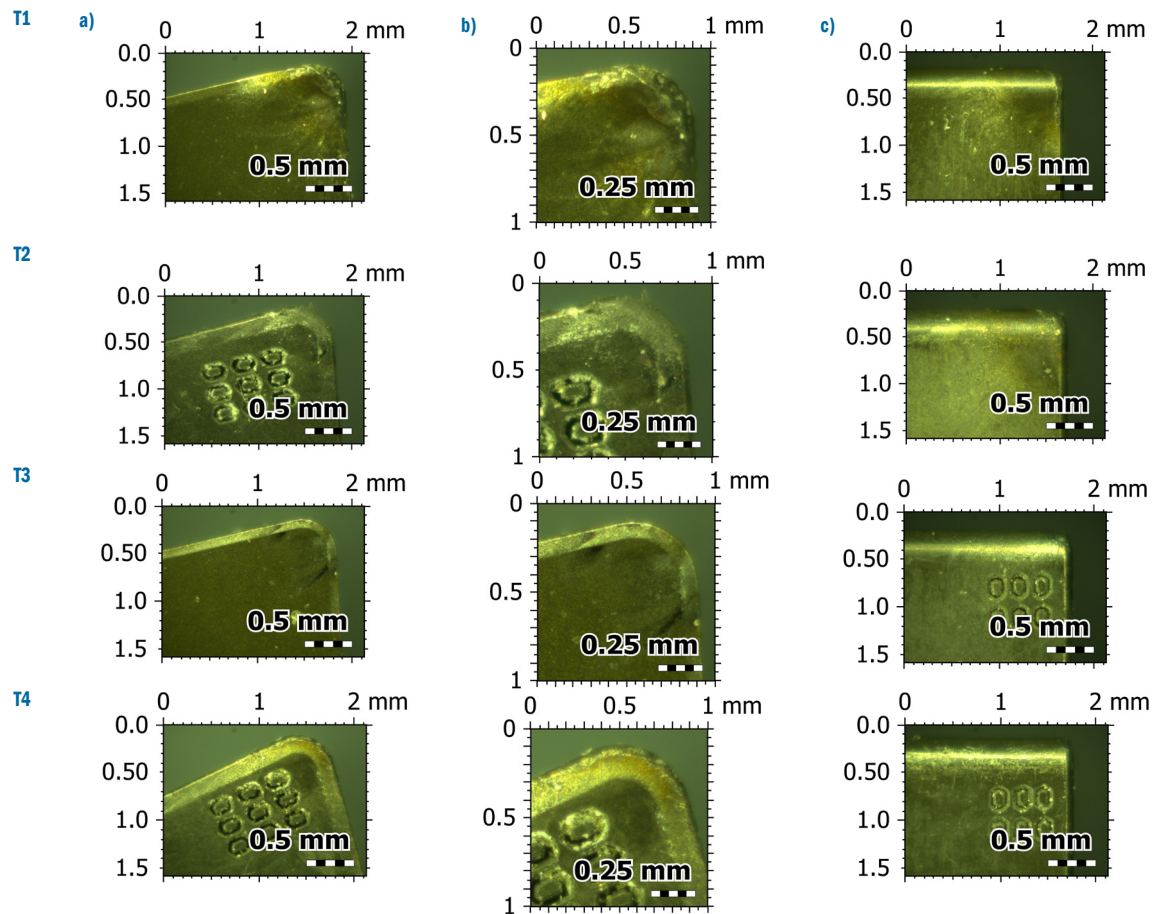


Fig. 19. SEM tool wear patterns of four types of cutting tools; a) front surface; b) local magnification; and c) side surface (all units in mm)

3.3 Influence of Lubricated Tools on Tool Wear

As shown in Fig. 16b, after excluding the maximum and minimum cutting forces, group 2 in the orthogonal test exhibits lower cutting forces. The corresponding tool wear under these conditions ($v = 800$ rpm, $f = 0.15$ mm/r, $a_p = 0.2$ mm) is depicted in Fig. 19, whereby r represents the number of revolutions per minute of the lathe spindle. For the conventional tool (T1), material tearing occurs, resulting in pits, scratches, and fracture marks on the tool surface. During continuous machining, the temperature at the tool-chip interface increases, leading to tip sintering and accelerated wear. The T3 tool undergoes mechanical plowing, where rough chip peaks embed into the tool surface under elevated temperatures, causing material displacement and sliding. In contrast, the microtexture structures of T2 and T4 promote efficient chip flow or partial embedding during extrusion, thereby reducing surface wear. The rear surface exhibits less wear compared to the front surface. Severe pit wear, scratching, and sintering are observed in T1, whereas T2, T3, and T4 display significantly reduced wear. The microtexture present on both tool surfaces effectively reduces friction. According to ISO 1993:3685 [23], Fig. 20 presents the tool flank wear after the turning tests, where VB is the wear width of the rear face. The measured wear widths before and after lubrication were 0.085 mm, 0.081 mm, 0.068 mm, and 0.062 mm respectively. Lubrication resulted in a 20 % to 24 % reduction in tool wear, demonstrating the effectiveness of solid lubricants in mitigating wear and prolonging tool life.

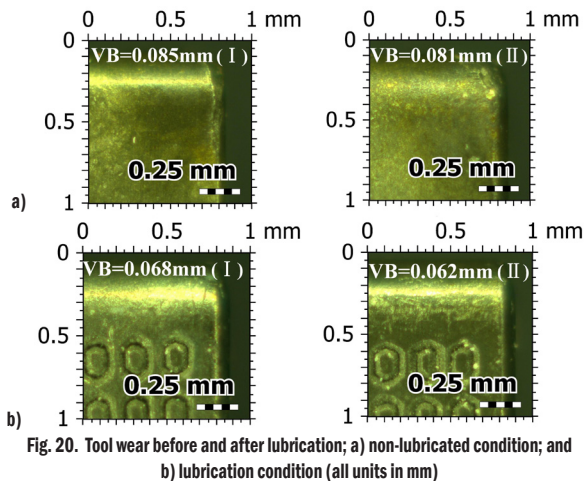


Fig. 20. Tool wear before and after lubrication; a) non-lubricated condition; and b) lubrication condition (all units in mm)

3.4 Influence of Lubricated Tools on Chip Formation

To facilitate clearer observation of the chip pattern, a larger feed rate and depth of cut were selected. Cutting tests were conducted under the conditions of $V = 800$ rpm, $f = 0.2$ mm/r, and $a_p = 0.5$ mm. The chip width and the average chip thickness were measured, along with the standard deviation for ten chip segments across four tool types. As illustrated in Fig. 21, conventional tools generate higher cutting forces, leading to severe deformation of the cutting layer and significant burr formation. Chips produced by conventional tools exhibit smaller curl radii and are less prone to breaking. During turning, curled chips were observed scratching the workpiece surface, adversely affecting machining accuracy. In contrast, under continuous cutting conditions, the microtextured tools effectively facilitate chip breaking. Fig. 22 shows that the actual chip thicknesses obtained from T1, T2, T3, and T4 exceeds theoretical values, with relative deviations of 14 %, 8 %, 11.5 %, and 7 %, respectively. This discrepancy arises due to plastic deformation along the shear line and friction compression in the secondary deformation zone, leading to chip accumulation. However, the microtextured tools mitigate chip

accumulation, producing chips with thicknesses closer to theoretical predictions.

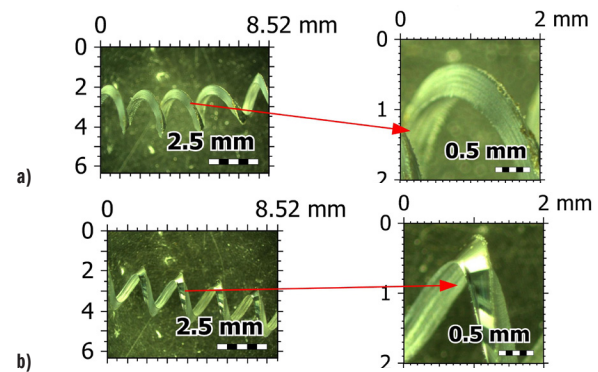


Fig. 21. Cutting chip morphology; shape; a) chip profile of the T1 tool under non-lubricated conditions; and b) chip profile of the T4 tool under lubricated conditions (all units in mm)

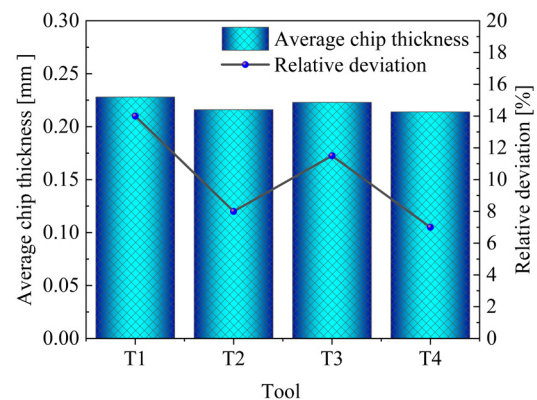


Fig. 22. Chip thickness and relative deviation for the four tool types

During the cutting process, the three distinct patterns of tool surface microtextures investigated in this study enhanced surface wettability. This improvement facilitated greater penetration of cutting fluid into the tool-chip interface, thereby establishing effective cooling and lubrication channels. The enhanced lubrication and heat dissipation within the cutting zone reduced frictional resistance between the tool and chip, resulting in diminished three-dimensional cutting forces and decreased tool wear. Additionally, the improved wettability promoted the removal of minute chips during tool-chip sliding friction, minimizing chip adhesion on the machined surface. Consequently, fewer surface defects, such as pits and scratches, were observed, resulting in improved surface integrity. Among the tools evaluated, the front and rear microtextured tools exhibited the highest wettability, providing superior cooling and lubrication, which contributed to the most substantial improvement in cutting performance.

4 CONCLUSION

To improve the cutting performance of turning tools, a novel PCBN microtextured composite tool has been proposed. The feasibility of the tool structure has been validated through turning tests. The following conclusions have been drawn:

1. Experimental and simulation data for the T4 tool have been compared, revealing an error in the range from 1 % to 7 %. This confirms the model's reliability and applicability for predicting cutting forces under specific conditions.
2. Under dry cutting conditions, the T4 tool demonstrated an average reduction of 19.8 % in cutting force compared to the T1

tool, indicating its superior cutting performance. The addition of solid lubricant further reduced the cutting forces of the T4 tool by an average of 6.41 %. These results underscore the significant improvement in cutting performance achieved through the combined effect of surface texturing and solid lubricants.

3. The T4 tool reduced workpiece surface roughness by 37.6 % compared to the T1 tool, while T3 and T2 achieved reductions of 30.6 % and 23.9 %, respectively. At a feed rate of $f = 0.15$ mm/r and depth of cut $a_p = 0.2$ mm, post-lubrication wear widths were 5.23 μ m for T1 and 3.86 μ m for T4, indicating wear reductions of 18.1 % and 19.5 % respectively. These results highlight the synergistic effect of solid lubricants and microstructures in improving surface quality and reducing tool wear.
4. The chip thickness for both T1 and T4 tools exceeded theoretical values due to compression and friction in the second deformation zone, leading to increased material accumulation. However, the T4 tool produced thinner chips than the T1 tool, as its surface microstructure facilitated chip fragmentation and reduced accumulation thickness.

Further research on microtextures with varying parameters and sizes, coupled with optimized cutting conditions and tool-workpiece material compatibility, could further enhance tool performance.

References

- [1] Ding, X., Liew, W.Y.H., Liu, X.D. Evaluation of machining performance of MMC with PCBN and PCD tools. *Wear* 259 1225-1234 (2005) DOI:10.1016/j.wear.2005.02.094
- [2] Persson, H., Filip Lenrick, Franca, L., Ståhl, J.E., Bushlya, V. Wear mechanisms of Pcbn tools when machining AISI 316L. *Ceram Int* 47 31894-31906 (2021) DOI:10.1016/j.ceramint.2021.08.075
- [3] Fan, L., Deng, Z., Gao, X., He, Y. Cutting performance of micro-textured PCBN tool. *Adv Mater Res-Switz* 4 023004 (2021) DOI:10.1063/1.50004372
- [4] Kishawy, H.A., Salem, A., Hegab, H., Hosseini, A., Balazinski, M. Micro-textured cutting tools: Phenomenological analysis and design recommendations. *CIRP Ann* 70 (2021) DOI:10.1016/j.cirp.2021.04.081
- [5] Patel, K., Kaftanoğlu, B., Özel, T. (2019). Micro textured cutting tool effects on cutting forces, volumetric wear and adhesion in dry turning of titanium alloy. *Int J Mech Manuf Syst* 12 180 DOI:10.1504/ijmms.2019.103482.
- [6] Pan, C., Li, Q., Hu, K., Jiao, Y. Song, Y. (2018). Study on surface roughness of gr15 machined by micro-texture PCBN tools. *Machines* 6 42 DOI:10.3390/machines6030042
- [7] Rajurkar, A., Chinchankar, S. Experimental investigation on laser-processed micro-dimple and micro-channel textured tools during turning of Inconel 718 alloy. *J Mater Eng Perform* 31 4068-4083 (2022) DOI:10.1007/s11665-021-06493-7
- [8] Li, Q., Pan, C., Jiao, Y., Hu, K. Investigation on cutting performance of micro-textured cutting tools. *Micromachines* 10 352 (2019) DOI:10.3390/mi10060352
- [9] Feng, Y., Zhang, J., Wang, L., Zhang, W., Tian, Y., Kong, X. Fabrication techniques and cutting performance of micro-textured self-lubricating ceramic cutting tools by in-situ forming of Al2O3-TiC. *Int J Refract Met H* 68 121-129 (2017). DOI:10.1016/j.ijrmhm.2017.07.007
- [10] Dai, L., Zheng, J., Dong, D., Sun, S., Liu, G. Effect of insert micro-texture types on the cutting force and temperature under various cooling conditions. *Int J Mechatr Manuf Syst* 14228-239 (2022) DOI:10.1504/ijmms.2021.121240
- [11] Wang, H., Meng, D., Wu, Z., Kang, J., She, D., Qin, W., Yue, W. Tribological behavior of polycrystalline cubic boron nitride sliding against WC-Co cemented carbide in vacuum conditions. *J Mater Eng Perform* 33 1975-1984 (2024) DOI:10.1007/s11665-023-08119-6
- [12] Kumar, C.S., Urbikain, G., De Lucio, P.F., Lopez de Lacalle, L.N., Pérez-Salinas, P., Gangopadhyay, S., and Fernandes, F. Investigating the self-lubricating properties of novel TiSiN coating during dry turning of Ti6Al4V alloy. *Wear* 532-533 205095-205095 (2023) DOI:10.1016/j.wear.2023.205095
- [13] Xing, Y., Luo, C., Zhu, M., Zhao, Y., Ehmann, K., Wu, Z., Liu, L. Assessment of self-lubricating coated cutting tools fabricated by laser additive manufacturing technology for friction-reduction. *J Mater Process Tech* 318 118010 (2023) DOI:10.1016/j.jmatprotec.2023.118010
- [14] Struzikiewicz, G. Investigation of the titanium alloy turning process with Prime A tools under high-pressure cooling conditions. *Stroj Vestn-J Mech E* 70 70-79 (2024) DOI:10.5545/sv-jme.2023.718
- [15] Korpysa, J., Kuczmazewski, J., Zagórski, I. Surface quality of AZ91D magnesium alloy after precision milling with coated tools. *Stroj Vestn-J Mech E* 69 497-508 (2023) DOI:10.5545/sv-jme.2023.651
- [16] Tamang, S.K., Chandrasekaran, M., Palanikumar, K., Arunachalam, R.M. Machining performance optimisation of MQL-assisted turning of Inconel-825 superalloy using GA for industrial applications. *Int J Mach Mach Mater* 21 43-65 (2019) DOI:10.1504/ijmmm.2019.098066
- [17] Ginting, A., Nouari, M., Bencheikh, I., Increasing productivity in hard turning of steels using CVD-coated carbide. *Int J Mach Mach Mater* 22 309-330 (2020) DOI:10.1504/ijmmm.2020.107060
- [18] Wang, Z., Wang, Y., Lv, D., Yu, X., Gao, Y. Performance and wear mechanisms of coated PCBN tools in high-speed turning superalloy GH4202. *Int J Adv Manuf Tech* 127 5083-5097 (2023) DOI:10.1007/s00170-023-11803-5
- [19] Maladen, R.D., Ding, Y., Li, C., Goldman, D.I. Undulatory swimming in sand: Subsurface locomotion of the sandfish lizard. *Science*, 325 314-318 (2009). DOI:10.1126/science.1172490
- [20] Ge, D., Deng, J., Duan, R., Liu, Y., Li, X., Yue, H. Effect of micro-textures on cutting fluid lubrication of cemented carbide tools. *Int J Adv Manuf Tech* 103 3887-3899 (2019) DOI:10.1007/s00170-019-03763-6
- [21] Gupta, M.K., Korkmaz, M.E., Sarıkaya, M., Krolczyk, G.M., Günay, M., Wojciechowski, S. Cutting forces and temperature measurements in cryogenic assisted turning of AA2024-T351 alloy: An experimentally validated simulation approach. *Measurement* 188110594 (2022) DOI:10.1016/j.measurement.2021.110594
- [22] Zhao, Z., Xie, X., Tang, G., Padhiar, M.A., Xiao, J., Liang, Z. Study on the effect of the strengthen grinding process surface coverage on the micro-morphology, micro-hardness, roughness, and residue stress of GCr15 bearing steels. *J Manuf Process* 99 362-372 (2023) DOI:10.1016/j.jmapro.2023.05.041
- [23] ISO 3685: 1993 (E). *Tool-life testing with single point tools* (1993)

Acknowledgements The authors would like to thank the members of the project team for their dedication and efforts, and the teachers and schools for their help. Here we need to thank the following organizations for their strong support "Project of Science and Technology Department of Jilin Province, Research on Key Technologies and Equipment Development for Riveting and Inspection of Automotive Brake piston Components: 20220201043GX".

Received 2024-10-02, revised 2025-01-20, 2025-02-15, 2025-03-09, accepted 2025-03-26 as Original Scientific Paper.

Data availability The data supporting the study's findings are included in the paper.

Author contribution Yan Zhang: conceptualization, formal analysis, writing – review & editing; Haodong Sun: writing – original draft, writing – review & editing, validation; Qi Li: validation, project administration; Yuanjing Mou: data curation; Kaiming Sun: data curation; Shihong Zhang: validation, supervision.

Raziskava rezalne učinkovitosti samomazivnih orodij z mikroteksturo sprednje in zadnje rezalne površine

Povzetek Študija obravnava implementacijo nove šestkotne mikroteksture za izboljšanje rezalne učinkovitosti orodij iz polikristalnega kubičnega borovega nitrida (PCBN). Razviti so tridimenzionalni modeli običajnih orodij in orodij z mikroteksturo, postopek struženja pa je simuliran s programsko opremo za končne elemente AdvantEdge. Preučeni so vplivi rezalne sile, temperature in napetosti na zmogljivost orodja. Rezultati kažejo, da se pri uporabi orodij z mikrostrukturami na sprednji in zadnji rezalni površini v kombinaciji s trdnimi mazivi rezalna sila zmanjša za 3 % do 7 %. Poleg tega se zmanjša koeficient trenja, izboljša se kakovost površine obdelovanca in poveča se odpornost površine orodja proti obrabi. Posledično orodja z mikrostrukturami v kombinaciji s trdnimi mazivi učinkovito izboljšajo rezalno zmogljivost.

Ključne besede šestkotna mikrostruktura, orodja PCBN, struženje, simulacija končnih elementov, integracija trdnih maziv